Calibration of Aperture Arrays in Time Domain Using the Simultaneous Perturbation Algorithm

Y. Zhang, *Member, IEEE,* H. Xing, X. Lv, M. Temiz, *Member, IEEE,* Y. Fu, Q. Shi, A. El-Makadema, A. Zhang, and J. Gao, *Senior Member*

***Abstract*—Online calibration is desired in antenna arrays of ultrawide bandwidth. This study proposes a time domain calibration method based on the simultaneous perturbation algorithm. Two objective functions were established: power of the received signal at array output; or combination of power and correlation coefficient between the signal at array output and a target signal. For both criteria, the convergence settings require only two measurements at each iteration. One advantage of the method is that the entire signal operation for calibration is performed in the time domain. This is achieved by resolving the effects of distortion on time delay of each channel, which accounts for both amplitude and phase distortions at different frequencies. Therefore, the proposed method significantly increased the calibration efficiency for ultra-wideband antenna arrays. Since time delay coefficients for calibration associated with array elements were determined independently due to characteristic of the simultaneous perturbation, estimation accuracy of the method is tangential to the number of elements in the array, and is mainly dependent on the convergence conditions. This gives the method an additional distinct advantage for calibrating large-scale antenna arrays with ultrawide bandwidth. An estimation accuracy of 99% on time delay adjustments has been achieved and demonstrated.**

***Index Terms*—aperture array, calibration, simultaneous perturbation (SP), stochastic approximation (SA), time domain**

I. Introduction

APERTURE arrays bring significant prospects and benefits for many applications as they enable steering of the radiation beams without any mechanical movement, therefore, they have better sensitivity, suppress the directional interference and incorporate multi-beam scanning [1], [2]. To maximize the array performance, a large number of array elements are often required and in order to accurately control the beam position, precise control of the phase and amplitude of each element is essential which, in turns requires accurate calibration, in order to eliminate unwanted distortions [3], [4]. However, calibration of large arrays becomes increasingly more challenging due to increasing number of parameters to be determined, particularly for very large-scale aperture arrays such as the Square Kilometre Array. This becomes even more challenging at higher operational frequencies for wider bandwidths, due to time delay drift at every array element becoming more sensitive to changes in the environment, and active radio frequency (RF) components. As a result, the number of measurements, in particular at on-site antenna assembly, on the objective function needed for calibration also rises significantly [5]–[8].

Stochastic Approximation (SA) has been considered to be an effective method for solving problems consisting of a large number of unknown parameters such as the problem faced in the calibration of large-scale antenna arrays [4], [9]. The "simultaneous perturbation" (SP) concept was later introduced to reduce the number of measurements required on the loss function or gradient per iteration for stochastic search algorithms [10], [11]. The SP is also shown to accelerate the convergence of the SA using the adaptive simultaneous perturbation (ASP) [12]. It leads to a more efficient adaptive algorithm than traditional finite difference methods and has a potential on a wide range of practical implementations. However its actual implementation has not been sufficiently successful, because it is extremely costly to estimate the gradients as a large number of loss function measurements involved in the case of gradient-free approach. In the gradient-based scenario, the calculation of gradient usually requires the full knowledge of the relationship between the parameters being optimized and the loss function. However, in the optimization process for some applications, gradient is not available or is difficult to compute, such as for array calibration. In [13], [14], a new simultaneous perturbation stochastic approximation (SPSA) consensus algorithm for distributed tracking under unknown-but-bounded disturbances is proposed, it is suitable for distributed problems to estimate time-varying parameters and compensate them.

Determining complex signals (consisting of amplitude and phase) from each array element and compensating the element-to-element variations due to imperfect conditions is the key objective of the array calibration process [15]. Effective phased array calibration methods are based on toggling element phases such that in-situ element fields can be measured. However, since these methods must measure not only amplitudes but also phases of the array responses, they are difficult to apply due to practical difficulties, such as large-scale antenna arrays with increased bandwidth where obtaining accurate phase measurements in real time is still extremely challenging. A novel amplitude-only measurement method was developed in [16]. However, it requires a large number of measurements to extract the calibration coefficients.

Conventionally, calibrating antenna arrays aims to achieve

Y. Zhang, H. Xing, X. Lv, Y. Fu, Q. Shi, A. Zhang and J. Gao are with the School of Transportation, Nantong University, Nantong, Jiangsu Province, 226019, China, the corresponding author: X. Lv, e-mail: lvxianyang@ntu.edu.cn

M. Temiz is with Department of Electronic and Electrical Engineering, University College London, London, WC1E 7JE, UK.

A. El-Makadema is with the Department of Electrical and Electronic Engineering, School of Engineering, The University of Manchester, Oxford Road, Manchester, M13 9PL, UK.

Manuscript received January 05, 2022; revised March 05, 2022.

the equalization of amplitude and phase for all antenna channels of the array in the frequency domain [17]. In the calibration process, the characteristics of the array are represented by a manifold vector, which consists of amplitudes as well as phases that occur due to the distance from the source to each element in the array. Once the calibration has been completed, the system produces a synthesis of the coherent signals at the array output. The simplest aperture array calibration technique strive to calculate the optimal phase shifts in all channels by maximizing the received power at the array output [18]. For example, the phase adaptive method was utilised to tune the phase-shifters, but this does not guarantee an optimal solution in antenna array calibration problem, even with high-resolution phase-shifting circuits [19].

More robust calibration algorithms using phase measurements reduce the implementation scope to laboratory conditions. The rotating element electric-field vector (REV) was developed in 1982, and since then a few modifications have been made to enhance its capability and it requires measurement at the element level [20]. The most recent calibration algorithms are the ones that do not require measurements at the element level. Hence, no or minimum disruption is caused to the array operation [18]. In these methods, finite number of power measurements at array output are carried out, the measured data are then used for estimating unknown phase shifts in order to compensate them for each channel. However, these algorithms are currently limited to narrow band systems as they are essentially implemented in the frequency domain.

There are many techniques developed, mostly in frequency domain, for array calibration. They were tentatively classified into six categories, and summarized in Table I. As indicated in the table, most of the calibration methods operate in the frequency domain. It can be seen in the table, the number of measurements required for the calibration are significantly high for some techniques, i.e., a few times more than the total number of elements in the array.

The SPSA has been proven to be an effective stochastic optimization method [10]. The biggest advantage of this method is that it is very effective when the loss function measurements include noise. In addition, it does not need gradient measurements on the loss functions. This method was initially proposed to solve multivariate optimization problems [11]. The method has attracted considerable attention due to its easy implementation. The underlying gradient approximation requires only two measurements of the loss function regardless of the dimension of the optimization problem. Random directions is another gradient search procedure [21], in which the perturbation variables are considered to be uniformly distributed over the surface of a unit sphere. However, it is computationally expensive to obtain the perturbation of random variables. Therefore, in this study, the SPSA approach was adopted as it can handle the optimization of a large number of variables without demanding prior information of gradients, as in the case of array calibration in time domain.

A novel calibration method in time domain is presented in this paper. This algorithm does not require to access channel signals or powering down channels for time delay estimation for each array element (signals from array elements are processed through channels in the receiver). The gradients in each iteration were approximated by a highly efficient and easily implemented "simultaneous perturbation," and only two measurements are required at each iteration. The total number of measurements is significantly reduced, which are required to resolve the time delay offset for each element of the array in compensation process. Using the same analogy, in addition to the power measurement approach, the correlation coefficient between the signal based on time delay perturbed element channels and the desired signal is used as a factor for objective function construction. Both forms of objective function in implementing the algorithm for array calibration are investigated in this study.

This is the first attempt to calibrate aperture arrays in the time domain by exploiting the SPSA method, to the best of the authors' knowledge. The proposed method not only avoids seeking calibration coefficients for a large number of frequency points required in wideband array calibrations, but also opens a new door for efficient calibration of arrays consisting of a large number of elements, such as the square kilometre array. By adopting the simultaneous perturbation technique, estimation errors on time delay distortions of element channels were controlled by a unified convergence criterion and are independent from each other. Hence, the total number of array elements has a negligible effect on accuracy. It is the number of iterations needed to reach convergence that rises with an increasing number of elements in the array and not the estimation error as will be outlined in Section V.

The paper is organized as follows: Section II gives the definitions of symbols used in this study. Section III describes the SA theories and convergence conditions; Section IV explains the proposed antenna array calibration method in the time domain; Section V makes numerical analysis on the algorithm; Section VI introduces the experiments, gives the results; Discussions on the algorithm are made in Section VII; finally, Section VIII presents the concluding remarks.

II. Symbols

This paper uses $\boldsymbol{T}$ and its variants as vectors representing time delays of element channels in arrays, and a variable with a hat means the value is obtained based on approximation, such as $\hat{\boldsymbol{g}}_k$ which is a vector consisting of approximated gradients at the kth step, further, $\mathbb{E}$ represents an expectation operator. Rationalized m.k.s units are used, the main symbols used in this study are defined as:

$\boldsymbol{s}(\boldsymbol{t})$ = short pulse signal in the time domain (volts)

$\sigma_p^2 \overset{def}{=}$ variance of the Gaussian pulse signal

$w \overset{def}{=}$ constant related to the time width of Gaussian pulse signal used for calibration

P_t = average power of the transmitted pulse signal (watts)

P_r = average power of the received signal from the array without calibration (watts)

$\boldsymbol{s}_m(\boldsymbol{t})$ = the signal received from the mth element (volts)

A_m = the amplitude gain for the mth element

ξ_m = the spatial time delay of the signal received by the mth element due to relative spacing, determined by scan angle and element spacing

$\boldsymbol{T}_{spatial} \stackrel{def}{=}$ vector of spatial time delay related to element spacing and scan angle, which is known to the system

γ_m = the intrinsic time delay generated in random for the mth element to reflect imperfect receiving condition, it is unknown to the algorithm

$\boldsymbol{T}_{in} \stackrel{def}{=}$ vector of the intrinsic time delays introduced in array element channels, representing impact by environment and imperfect devices, the values in this vector are the time delays to be calibrated out by the algorithm

$\boldsymbol{T} \stackrel{def}{=}$ vector of time delays for all elements including spatial time delays and time delays caused by the imperfect receiving condition

τ_m = the approximated time delay of mth element representing the misalignment of timing between elements, the time delay approximated by the algorithm for calibration

$\hat{\boldsymbol{T}}^{*} \stackrel{def}{=}$ vector of optimal calibration coefficients of time delay for all element channels approximated by the algorithm

$\boldsymbol{T}_0^{*} \stackrel{def}{=}$ vector of the initial guess of time delays of all elements at the beginning of approximation process

$\hat{\boldsymbol{T}}_k \stackrel{def}{=}$ vector of estimated calibration coefficients of time delay at the kth iteration

$P_k \stackrel{def}{=}$ power received at array output when the array is calibrated with coefficients from approximation at the kth step

$P_{ideal} \stackrel{def}{=}$ the ideal power received at array output when there is no time delay distortions in the element channels

$\boldsymbol{s}_b(\boldsymbol{t}) \stackrel{def}{=}$ the received signal at the array output when the backward time perturbation is applied

$\boldsymbol{s}_f(\boldsymbol{t}) \stackrel{def}{=}$ the received signal at the array output when the forward time perturbation is applied

$P_b \stackrel{def}{=}$ the measured output power when the backward perturbation is applied

$P_f \stackrel{def}{=}$ the measured output power when the forward perturbation is applied

$l_b \stackrel{def}{=}$ loss function value when the backward perturbation is applied

$l_f \stackrel{def}{=}$ loss function value when the forward perturbation is applied

$l \stackrel{def}{=}$ the scalar loss function determined by the power received at the array output alone, or the product of power and the correlation coefficient between the signal from array output and the ideal reference signal for calibration

a_k = the gain coefficient for the kth iteration

c_k = the perturbation step coefficient for the kth iteration

$\Delta_{ki} \stackrel{def}{=}$ the ith element of vector $\boldsymbol{\Delta}_k$ with the total length of M, k is the current iteration number

$\boldsymbol{\Delta}_k \stackrel{def}{=}$ the perturbation vector with the total length of M, each element of the vector is generated using a Bernoulli distribution with probability of 0.5 for ± 1

$\hat{\boldsymbol{g}}_k(\hat{\boldsymbol{T}}_k) \stackrel{def}{=}$ the approximated gradients vector at the kth iteration of the algorithm

$r(\mathbf{x}, \mathbf{y})$ = correlation coefficient between the vector $\mathbf{x}$ and vector $\mathbf{y}$

III. Stochastic approximation theories

To identify the appropriate SA algorithms for array calibrations, convergence condition is an important factor to consider. In this section, we give a brief review of SA theories and their corresponding convergence conditions.

The basic stochastic approximation algorithm is essentially a stochastic difference equation with a small step size, and the prime concern is its qualitative behavior after many iterations, such as convergence and rate of convergence. Proofs of convergence and the derivation of the rate of convergence have been given for a variety of equations and stochastic processes over a period of several decades. In early development of stochastic search and optimization—Stochastic Approximation (SA), the Robbins-Monro algorithm (also known as RM) for root-finding is the basic approach. Recursive procedure for finding the root of a real-valued function $g(\theta)$ was developed. Suppose that the values of $g(\theta)$ was not known, but "noise corrupted" observations can be taken with respect to the values of θ. By proposing

$$\theta_{k+1} = \theta_k + a_k Y_k, \tag{1}$$

where a_k is an approximate gain sequence satisfying

$$a_k > 0,\ a_k \to 0,\ \sum_{k=0}^{\infty} a_k = \infty, and\ \sum_{k=0}^{\infty} a_k^2 = \infty, \tag{2}$$

and Y_n is the noisy estimation of the value $g(\theta)$. The decreasing step sizes a_k would provide an implicit averaging of the observations and are essential to ensure convergence for this algorithm.

For another type of basic problems, to seek the value of the variable at the minimum of a smooth function—sometimes—the form of the function is unknown such as for an array calibration problem, instead "noise corrupted" observations or measurements can be obtained, then the Kiefer–Wolfowitz procedure (a.k.a KW algorithm) can be used, in which gradients for directing the recursive computation are estimated via finite differences using the noisy measurements, and the step sizes are also small. Assume the value of parameter θ is to be found for the function $EF(\theta, \boldsymbol{\chi}) = f(\theta)$, where $f(\cdot)$ is continuously differentiable and $\boldsymbol{\chi}$ is a random vector, the functions $F(\cdot)$ and $f(\cdot)$ are not known and loosely speaking, $f(\theta)$ is an "estimator" of $F(\theta, \boldsymbol{\chi})$. Let $c_k \to 0$, finite difference can be expressed as [43]

$$Y_k = -\frac{F\left(\theta_k + c_k, \boldsymbol{\chi}_k^{+}\right) - F\left(\theta_k - c_k, \boldsymbol{\chi}_k^{-}\right)}{2c_k} \tag{3}$$

and the iteration can be established as

$$\theta_{k+1} = \theta_k + a_k Y_k, \tag{4}$$

where Y_k can be estimated by

$$\gamma_k \equiv \frac{f(\theta + c_k) - f(\theta - c_k)}{2c_k} = f_\theta(\theta_k) - \beta_k, \tag{5}$$

where -β_k is the bias in the finite difference estimation $f_\theta(\theta_k)$. Accordingly, the iteration relation can be updated as

$$\theta_{k+1} = \theta_k - a_k f_\theta(\theta_k) + a_k \frac{\psi_k}{2c_k} + a_k \beta_k, \tag{6}$$

where ψ_k is the finite difference between the estimated $f(\theta)$ and the actual $F(\theta, \boldsymbol{\chi})$ when θ changes from θ+c_k to θ-c_k. To ensure convergence, in addition to the condition for the bias,

This article has been accepted for publication in IEEE Transactions on Antennas and Propagation. This is the author's version which has not been fully edited and content may change prior to final publication. Citation information: DOI 10.1109/TAP.2023.3255642

TABLE I
SELECTED TYPICAL CALIBRATION METHODS

Calibration Methods		Domain	Measurement	Notes
Field Measurement	Near-field probing [22]–[25]	Frequency Domain	Amplitude, Phase	Difficult to measure
	Direct measurement [5], [7], [26], [27]	Frequency Domain	Amplitude, Phase	Difficult to measure
MCM	Mutual Coupling Measurement [28], [29]	Frequency Domain	Amplitude, Phase	M measurements
MEP	Phase-toggle method [30], [31]	Frequency Domain	Amplitude, Phase	Numerous probe scanning
REV	Classical REV [20], [32], [33]	Frequency Domain	Power	7M+1
	Extended REV [15], [34]	Frequency Domain	Power	Depend on grouping strategy
	Improved REV [35]	Frequency Domain	Power	Depend on grouping strategy
Phase adaptation	Adaptive algorithm [9], [36]	Frequency Domain	Power	6(M-1)+2 measurements
	Perturbation algorithm [18], [19]	Frequency Domain	Power	6(M-1)+1 measurements
	FPC(Four-Phase-Cycle) [17], [37]	Frequency Domain	Power	4(M-1) measurements
	Three-Phase-Cycle [38]	Frequency Domain	Power	2M+1
Self-calibration	Self-calibration [39], [40]	Frequency Domain	Mutual Coupling/Patterns	using iterations
CS	Compressed sensing [41], [42]	Frequency Domain	Patterns	using iterations

$\beta_k \to 0$, the noise term $\psi_k/(2c_k)$ is also required to go towards zero (through "average locally.") The KW algorithm, when the noisy estimates of the derivatives are available, are generally based on the these derivatives to direct the recursions towards a converged result. For the same minimization problem, when the stochastic gradient is not available, and only measurements of loss function are available, a finite-difference (FD) approximation to the gradient is proposed. The FD approximation relies on a small change on the variable θ, the value of loss function is then measured. However, the FD-based SA (FDSA) algorithm can be very costly when the dimension p of the variables is high for we have to measure at least once for each variable to be optimized. With two-sided perturbations, $2p$ measurements are required in each recursion. The recursive procedure can be expressed in the general SA form [44]

$$\hat{\boldsymbol{\theta}}_{k+1} = \hat{\boldsymbol{\theta}}_k - a_k \hat{\boldsymbol{g}}_k(\hat{\boldsymbol{\theta}}_k), \tag{7}$$

where $\hat{\boldsymbol{\theta}}_k$ and $\hat{\boldsymbol{g}}_k$ are two vectors consisting of the variables for optimization and the corresponding gradient approximations respectively. The FDSA gradient approximation can be expressed as

$$\hat{\boldsymbol{g}}_k(\hat{\boldsymbol{\theta}}_k) = \begin{bmatrix} \frac{f(\hat{\boldsymbol{\theta}}_k + c_k \boldsymbol{\xi}_1) - f(\hat{\boldsymbol{\theta}}_k - c_k \boldsymbol{\xi}_1)}{2c_k} \\ \frac{f(\hat{\boldsymbol{\theta}}_k + c_k \boldsymbol{\xi}_2) - f(\hat{\boldsymbol{\theta}}_k - c_k \boldsymbol{\xi}_2)}{2c_k} \\ \vdots \\ \frac{f(\hat{\boldsymbol{\theta}}_k + c_k \boldsymbol{\xi}_p) - f(\hat{\boldsymbol{\theta}}_k - c_k \boldsymbol{\xi}_p)}{2c_k} \end{bmatrix}, \tag{8}$$

where $\boldsymbol{\xi_i}$ represents a vector with a 1 in the ith place the 0's for the rest, and $c_k > 0$ defines the steps for changes. The pair (a_k, c_k) are the gain sequences for the FDSA algorithm. Compared to the convergence theory for the root-finding RM algorithm, the conditions for convergence of the FDSA algorithm (evolved from KW algorithm) have an extra gain sequence c_k, arising from the bias in $\hat{\boldsymbol{g}}_k(\hat{\boldsymbol{\theta}})$ as an estimator for $\boldsymbol{g}_k(\hat{\boldsymbol{\theta}})$. The conditions for the formal convergence (almost sure, a.s.) of the FDSA algorithm are as follows [44]

- **A.1** **(Gain sequences)** $a_k > 0$, $c_k > 0$, $a_k \to 0$, $c_k \to 0$, $\sum_{k=0}^{\infty} a_k = \infty$, and $\sum_{k=0}^{\infty} a_k^2/c_k^2 < \infty$.
- **A.2** **(Unique minimum)** There is a unique global minimum point of $\boldsymbol{\theta}^*$, away from this point, $f(\boldsymbol{\theta})$ will always increase.
- **A.3** **(Mean-zero noise and finite variance noise)** The standard mean-zero and bounded variance noise condition.
- **A.4** **(Smoothness of the loss function)** The second derivatives of the function $f_{ii}^{''}(\boldsymbol{\theta})$ exist and are uniformly bounded.

Clearly, a large number of measurements ($2p$ times the total number of iterations) are required when p is large. Hence, SPSA algorithm came into attention, where the required measurements can be significantly reduced by approximating the gradients for all variables simultaneously at each iteration. The gradient approximation for SPSA is generated by

$$\hat{\boldsymbol{g}}_k(\hat{\boldsymbol{\theta}}_k) = \frac{f(\hat{\boldsymbol{\theta}}_k + c_k \boldsymbol{\Delta}_k) - f(\hat{\boldsymbol{\theta}}_k - c_k \boldsymbol{\Delta}_k)}{2c_k} \begin{bmatrix} \Delta_{k1}^{-1} \\ \Delta_{k2}^{-1} \\ \vdots \\ \Delta_{kM}^{-1} \end{bmatrix}. \tag{9}$$

In contrast to the FDSA algorithm, with simultaneous perturbation, two loss measurements are needed in each approximation cycle instead of $2p$, regardless of the dimension p. The convergence conditions of SPSA algorithm are closely related to that of the FDSA algorithm, in addition to a more stringent requirement on smoothness of the loss function, i.e., three-times differential, two more conditions are added.

- **B.1** **(Measurement noise; relationship between measurement noise and $\boldsymbol{\Delta}_k$)** This condition together with smoothness of the loss function guarantee the gradient estimate $\hat{\boldsymbol{g}}_k(\hat{\boldsymbol{\theta}})$ is an unbiased estimate of $\boldsymbol{g}_k(\hat{\boldsymbol{\theta}})$ in the order of $O(c_k^2)$.
- **B.2** **(Statistical properties of the perturbations)** The bounded inverse moments condition for the Δ_{ki} is an important part of SPSA, the symmetric Bernoulli distribution ± 1 satisfies the inverse moments, which ensures $\hat{\boldsymbol{g}}_k(\hat{\boldsymbol{\theta}})$ is a nearly unbiased estimate of $\boldsymbol{g}_k(\hat{\boldsymbol{\theta}})$.

As pointed out in [44], proofs of the convergence theorems for the FDSA and SPSA have been provided by Fabian (1971), Spall (1992), Dippon and Renz (1997), etc. The convergence conditions mentioned above illustrate an abstract idea. For solving real problems such as array calibration in this study, we gave specific loss function definitions and checked the convergence conditions for arrays with various number of elements. The strategy of selecting optimal parameter coefficients in the algorithm for effective convergences have been studied considering implementations in practice.

IV. The Proposed Calibration Method

Due to the growing demands of high-speed communication and high-precision sensing applications, ultra-wideband antenna arrays operating at millimeter wave or THz frequencies have become increasingly more important. It is more efficient to carry out calibration for such arrays in the time domain. As mentioned earlier the method based on simultaneous perturbation in conjuncture with a deterministic approach was proven to be effective in the frequency domain. In this paper, the SPSA method is implemented in the time domain for the first time. Fig. 1 shows the setting to calibrate an antenna array with M elements in the time domain. The proposed calibration method is put to a test by employing a short pulse signal in the time domain illuminating the aperture array being measured in a known plane wave. It should be noted that although the calibration waveform is known, the delay between the antenna for transmitting the source signal and the antenna elements of array are not exactly known owing to the parasitic random time delays that is caused by the imperfect receiving components and propagation environment. Therefore, the proposed calibration algorithm strives to perform fine tracking on the time delay in each channel and compensate them before acquisition of the received signals at array output.

Let $\boldsymbol{s(t)}$ denote a time domain signal which is a Gaussian pulse as given by

$$\boldsymbol{s(t)} = \frac{1}{4\sqrt{2\pi\sigma_p^2}} e^{\frac{-w^2\boldsymbol{t}^2}{2\sigma_p^2}}, \tag{10}$$

where σ_p^2 denotes the variance of the Gaussian pulse and w controls the time width. This pulse signal propagated from a transmitter in the far-field of an aperture array to be calibrated. The average power of the transmitted pulse signal for calibration can be expressed by

$$P_t = \mathbb{E}\left\{|\boldsymbol{s(t)}|^2\right\}. \tag{11}$$

Subsequently, the signal received by the mth element of the aperture array before calibration and the synthesizer can be represented by

$$\boldsymbol{s}_m(\boldsymbol{t}) = A_m \boldsymbol{s}(\boldsymbol{t} - \xi_m - \gamma_m), \tag{12}$$

where A_m denotes the channel gain between the transmitter of reference and the mth antenna element, consisting of antenna gains and path-loss. Moreover, ξ_m denotes the spatial time delay of the signal received by the mth element associated with physical distance, and γ_m denotes the intrinsic time delay (generated randomly) introduced by other factors from devices

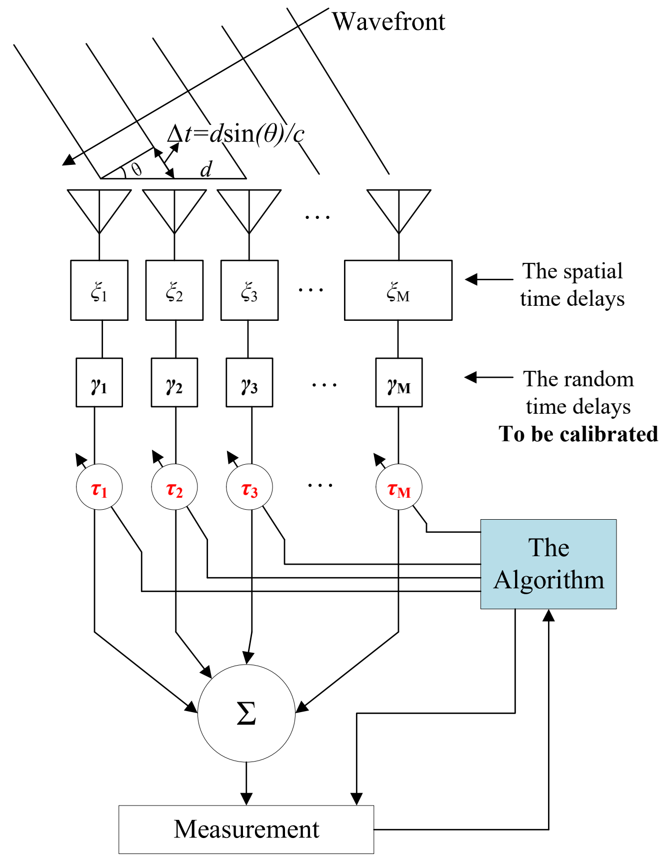

Fig. 1. Calibration of aperture arrays in the time domain based on the SPSA algorithm.

and environment. Therefore, the vector $\boldsymbol{T}_{spatial}$ consisting of time delays for M elements is defined as

$$\boldsymbol{T}_{spatial} = [\xi_1, \xi_2, \cdots, \xi_m, \cdots, \xi_M]. \tag{13}$$

For example, when the angle of incidence, $\theta = 30°$, and the element spacing of $d = 0.015$ m, $\boldsymbol{T}_{spatial} = [0, 0.025, \cdots, 0.375]$ for $M = 16$. Random time delays are introduced into each channel to represent the imperfect array construction or distortion caused by the receiver devices, as given by,

$$\boldsymbol{T}_{in} = [\gamma_1, \gamma_2, \cdots, \gamma_m, \cdots, \gamma_M]. \tag{14}$$

where γ_m can be generated by $\gamma_m = 2x - 1$ and is in the interval (-1,1) and x = rand(1) is a uniformly distributed random number in the interval (0,1). The interval for γ_m can be adjusted to reflect the actual time delay distortions in real systems. Consequently, the vector of the actual time delays for all channels can be expressed by

$$\boldsymbol{T} = \boldsymbol{T}_{spatial} + \boldsymbol{T}_{in}. \tag{15}$$

Let the sampling frequency for the time domain signal be f_s, and hence, the time resolution of the signal is given by

$$dt = \frac{1}{f_s}. \tag{16}$$

Assuming the total length of the time domain signal in a processing frame for any channels is L, and M is the total number of array elements, then the average received power from the array without calibration can be calculated by

$$P_r = \mathbb{E}\left\{\left|\sum_{m=1}^{M} \boldsymbol{s}_m(\boldsymbol{t})\right|^2\right\}. \tag{17}$$

The respective time of arrival for the signal received in each channel varies with imperfect array construction and/or other factors. Hence, the synthesized signal in the array receiver without calibration is significantly different from that after all element channels are calibrated.

In order to make an approximation on the objective vector of time delays for calibration, $\hat{\boldsymbol{T}}^*$, which is used to compensate for the random time delays occurring in the antenna array system within each channel, $\boldsymbol{T}_{in}$, and $\hat{\boldsymbol{T}}^*$ is defined as

$$\hat{\boldsymbol{T}}^* = [\tau_1, \tau_2, \cdots, \tau_m, \cdots, \tau_M], \tag{18}$$

where τ_m $(m = 1, 2, 3, \cdots, M)$ denotes the approximated time delay calibration coefficient for the element m.

The SPSA algorithm has been designed to estimate the distorted time delay in each element channel. Since there are many receiving elements in the array, the problem of calibration has been converted into a multivariate stochastic search and optimization problem. The key problem for the algorithm to address is to seek the values of variants to minimize the value of a loss function. The loss function is crucial for the calibration performance and can be defined in different ways. More detailed description on loss function definition will be presented in Section V. To illustrate the renewed steps of the SPSA algorithm for array calibration, tentatively, the loss function was assumed to be related to power at array output, it can be defined as:

$$l = 1 - \frac{P_k}{P_{ideal}}, \tag{19}$$

where P_k is the average power measured at the array output when $\hat{\boldsymbol{T}}_k$ is used to compensate the time distortions, $\boldsymbol{T}_{in}$, and P_{ideal} is the desired power at array output when the time distortions in the element channels are fully eliminated. The step-by-step description below shows how the simultaneous perturbation algorithm was implemented for aperture array calibration in the time domain.

Step 1 Initialization and set up algorithm coefficients for perturbation. Then set time of arrival of impinging signals for each channel due to difference in propagation path length, $\boldsymbol{T}_{spatial}$. Then select the coefficient constants before iteration begins, and generate the random time delay vector representing the imperfect channel condition, $\boldsymbol{T}_{in}$.

Step 2 Generation of simultaneous perturbation vector, a M-dimensional random perturbation vector $\boldsymbol{\Delta}_k$, the time delays for all channels in each iteration are decided by the random perturbation vector and the coefficients chosen at the beginning, a simple choice of the perturbation vector is to use a Bernoulli distribution with probability of 0.5 for each ± 1 outcome. An example of $\boldsymbol{\Delta}_k$ is $\boldsymbol{\Delta}_k = [-1, 1, \cdots, -1]$.

Step 3 Power measurements at the array output and evaluations, obtain two measurements from the power calculation function as shown in (17) based on the simultaneous perturbation around the time delays for the current iteration, k, $l(\hat{\boldsymbol{T}}_k$+$c_k\boldsymbol{\Delta}_k)$ and $l(\hat{\boldsymbol{T}}_k$-$c_k\boldsymbol{\Delta}_k)$.

Step 4 Gradient approximation, generate the simultaneous perturbation approximation to the unknown gradients

$$\hat{\boldsymbol{g}}_k(\hat{\boldsymbol{T}}_k) = \frac{l(\hat{\boldsymbol{T}}_k + c_k\boldsymbol{\Delta}_k) - l(\hat{\boldsymbol{T}}_k - c_k\boldsymbol{\Delta}_k)}{2c_k} \begin{bmatrix} \Delta_{k1}^{-1} \\ \Delta_{k2}^{-1} \\ \vdots \\ \Delta_{kM}^{-1} \end{bmatrix}. \tag{20}$$

where Δ_{ki} is the ith component of the $\boldsymbol{\Delta}_k$ vector with the total length of M, and $\boldsymbol{\Delta}_k$ is given in Step 2. It is noted that the denominator is the same for all components of $\hat{\boldsymbol{g}}_k$ vector within one iteration, and reflects the characteristics of the simultaneous perturbation in contrast to other approximation methods.

Step 5 Updating the time delay estimate, use the SA form to calculate the time delays for the following iteration step.

$$\hat{\boldsymbol{T}}_{k+1} = \hat{\boldsymbol{T}}_k - a_k\hat{\boldsymbol{g}}_k(\hat{\boldsymbol{T}}_k). \tag{21}$$

Step 6 Repeat from Step 2 for more iterations or terminate, terminate the algorithm if the condition is met such as, $l \leq \sigma$, and l is the loss function as defined in (19), or set a limit for the maximum number of iterations.

V. NUMERICAL ANALYSIS

This section presents the detailed steps including objective function definitions, coefficients selection strategies, and performance analysis of the proposed calibration algorithm. It was examined for calibration of aperture arrays consisting of various number of elements aiming for different levels of accuracy. Once the objective function is defined, the strategy of giving values to the optimization coefficients a_k and c_k is essential for a successful convergence.

The study began with the following assumptions. The source signal given by (10) with 1 ns duration impinged on the planar surface of the aperture array with a particular angle of incidence from a point at far field, and the time of arrival for the signal received on each element varies with the relative distance among elements. The time delays related to the relative distance were calculated by using the parameters including angle of incidence and the element spacing. Furthermore, the time delay on each channel is distorted by a combination of many factors including Tx/Rx module impairments, feed circuit variations, mutual coupling, and diffraction due to antenna structures. In the simulation, time delay distortion in each channel is collectively represented by a vector of random numbers, $\boldsymbol{T}_{in}$, subject to Gaussian distribution with zero mean and within a specified time range.

Definition of the loss function is critically important for the proposed algorithm to be successfully implemented as the outcome of approximation heavily depends on it. Two loss function options were explored in this work: power measurement based objective function; product of power measurement and correlation coefficient calculation at array output. The following analysis was made to provide a general guidance

This article has been accepted for publication in IEEE Transactions on Antennas and Propagation. This is the author's version which has not been fully edited and content may change prior to final publication. Citation information: DOI 10.1109/TAP.2023.3255642

Algorithm 1 Calibration of Aperture Array in the time domain with Simultaneous Perturbation

Input: input parameters M, $\boldsymbol{T}_{spatial}$, $\boldsymbol{s}(\boldsymbol{t})$
Output: $\hat{\boldsymbol{T}}^*$

1: Signal initialization for each channel with specified delays defined by the scan angle and element spacing
2: Assign values to the perturbation constants, a, c, A
3: Generate the random time delays in each channel, $\boldsymbol{T}_{in}$, it represents time delays in the imperfect channels, they are to be calibrated out by the algorithm
4: Calculate the power of the synthesized signal when the time delay distortions are hypothetically eliminated, P_{ideal}
5: Make the first guess on the time delays in each channel, $\boldsymbol{T}_0^*$, let $k=1$
6: **while** $l > \sigma$ **do**
7: Generate the simultaneous perturbation vector, $\boldsymbol{\Delta}_k$
8: Sum up the signals from each channel for two separate time delays after applying the simultaneous perturbation, the synthesized signal at array out with backward perturbation, $\boldsymbol{S}_b(\boldsymbol{t}) = \sum_{m=1}^{M} \boldsymbol{s}_m(\boldsymbol{t} + \xi_m + \hat{\boldsymbol{T}}_k(m) + c_k \Delta_{km})$, whereas with the forward perturbation applied in each element channel, the synthesized signal at array output is $\boldsymbol{S}_f(\boldsymbol{t}) = \sum_{m=1}^{M} \boldsymbol{S}_m(\boldsymbol{t} + \xi_m + \hat{\boldsymbol{T}}_k(m) - c_k \Delta_{km})$
9: Obtain the two power measurements with the respective time perturbations, $P_b = \mathbb{E}\left\{|\boldsymbol{S}_b(\boldsymbol{t})|^2\right\}$, $P_f = \mathbb{E}\left\{|\boldsymbol{S}_f(\boldsymbol{t})|^2\right\}$, and then let $l_b = 1 - \frac{P_b}{P_{ideal}}$, $l_f = 1 - \frac{P_f}{P_{ideal}}$
10: Calculate the gradient vector for the current, the kth, iteration based on the two power measurements from the last step, the gradient vector is, $\hat{g}_k(\hat{\boldsymbol{T}}_k) = \frac{l_f - l_b}{2c_k} \begin{bmatrix} \Delta_{k1}^{-1} \\ \Delta_{k2}^{-1} \\ \vdots \\ \Delta_{kM}^{-1} \end{bmatrix}$
11: Calculate the time delay adjustment vector for the next iteration, $\hat{\boldsymbol{T}}_{k+1} = \hat{\boldsymbol{T}}_k - a_k \hat{\boldsymbol{g}}_k(\hat{\boldsymbol{T}}_k)$, let $k = k+1$
12: **return** Time delay offset for each channel, $\hat{\boldsymbol{T}}^* \cong \hat{\boldsymbol{T}}_k$

on efficient implementation of the array calibration method in the time domain based on the SPSA algorithm.

A. Power measurement based objective function

The objective function can be decided by the received power at array output as defined in (19). The guidelines from the basic SPSA algorithm for coefficients selection were tested for the specific array calibration problem and presented below, but it had been warned that they are guidelines only—may not be the best or even work for every application. In this section, new coefficients selection strategies for effective array calibrations were established and compared with that based on the guidelines from the basic SPSA algorithm.

The first guess of time delay coefficients to initiate the calibration process can be expressed as,

$$\boldsymbol{T}_0^* = \left[\tau_{0,1}, \tau_{0,2}, \cdots, \tau_{0,m}, \cdots, \tau_{0,M}\right]. \tag{22}$$

In order to estimate the magnitude of variations of the loss function at the beginning of the search, the power measurements can be obtained through several sets of $\boldsymbol{T}_0^*$ vectors with its components formed by randomly generated time delays within each channel. The corresponding values for the loss function are calculated by using (19) and arranged in a vector.

1) Basic SPSA guidelines: As shown in the guidelines of the SPSA method by J. C. Spall, the choice of these two parameters is related to the specific application of the algorithm, particularly, the magnitudes of the parameters which are to be optimized, i.e., the distorted time delays in each channel for the problem considered in this paper. Initial values of a_k and c_k are suggested in [11] by

$$a_k = \frac{a}{(A+k+1)^{\alpha}}, \tag{23}$$

and

$$c_k = \frac{c}{(k+1)^{\gamma}}, \tag{24}$$

where a, c, A, α and γ are the non-negative coefficients and can be selected before the optimization iterations begin. Initial values of α and γ are chosen at 0.602 and 0.101 as suggested in [11]. It was recommended that the parameter c can be approximately equal to the standard deviation of measurement noise. It can be estimated by using the variation of the loss function magnitudes that can be obtained by giving several guessed values to the parameters to be optimized.

To reach convergence effectively, prior to implementing iterations, initialization coefficients for the algorithm have to be selected with care as they depend on applications. The following subsection addresses the unique coefficient selection process concerning array calibration problems.

2) Optimal initialization coefficients selection: Recall that the relationship between a_k and c_k must ensure the convergence condition, i.e., $\sum_{k=0}^{\infty} a_k^2/c_k^2 < \infty$, let the ratio between them simply be

$$b_k = \frac{a_k}{c_k}, \tag{25}$$

and the values of b_k were closely observed during estimation steps to ensure convergence. It is delicate to prevent b_k from decaying too fast with an increasing k while maintaining a certain rate of change.

At the early iterations, it is important to keep the change of time delays under control. Before iterations begin, several guessed values can be given to $\boldsymbol{T}_0^*$ to evaluate the magnitude of loss function, approximated gradients, together with the desired magnitude of change in time delay at early iterations, initialization coefficients can be determined. The detailed procedure to calculate the initialization coefficients based on guesses on $\boldsymbol{T}_0^*$ was presented in Table II and Table III. Consequently, a_k and c_k can then be calculated at each iteration according to (23) and (24). It is noted that the optimal value of a_k is related to magnitude of the loss function, and c_k must be small enough to ensure that the perturbation is within the allowed range of the parameters to be optimized, i.e., the maximum possible time distortion in the system. Therefore, the values of the $\hat{\boldsymbol{g}}_k$ have to be closely monitored.

The algorithm terminates when the difference in measured power at the current iteration and the desired power at array output is close to each other. However, the solution to resolve the time delays based on power measurement alone may need a large number of iterations to converge. Therefore, the scenario—loss function based on product of power and correlation coefficient was introduced as another alternative to calculate gradients and establish the termination condition of the algorithm. This will be analyzed in the next section.

B. Correlation coefficient related objective function

As is shown in the previous section, an objective function based on power measurements as the termination condition for the algorithm requires a large number of iterations to reach convergence. Therefore, an objective function was proposed with an extra parameter—correlation coefficient is introduced to indicate and quantify the similarity of two signals in the time domain. Correlation coefficient is defined to analyze the similarity between two vectors, and given by $\mathbf{x} = [x_1, x_2, \cdots, x_l, \cdots, x_L]$ and $\mathbf{y} = [y_1, y_2, \cdots, y_l, \cdots, y_L]$, as

$$r(\mathbf{x}, \mathbf{y}) = \frac{\sum_{l=1}^{L}(x_l - \bar{x})(y_l - \bar{y})}{\sqrt{\sum_{l=1}^{L}(x_l - \bar{x})^2}\sqrt{\sum_{l=1}^{L}(y_l - \bar{y})^2}}, \tag{26}$$

where $\bar{x}$ and $\bar{y}$ denote the means of vector $\mathbf{x}$ and $\mathbf{y}$, respectively. During the approximation process, $r(\mathbf{x}, \mathbf{y})$ can be calculated by assuming $\mathbf{x}$ is the synthesized signal from the array output with an ideal receiving condition (i.e., the optimal signal desired at the array output), and the $\mathbf{y}$ is the synthesized signal vector from the array output when the time offset coefficients, $\hat{\boldsymbol{T}}_k$, is applied in element channels. The new objective function with an extra factor of correlation coefficient as an indicator for convergence testing is defined as,

$$l = 1 - r \times \frac{P_k}{P_{ideal}}. \tag{27}$$

when the objective function l approaches zero, the synthesized signal at the array output with the corrected time delay for each channel becomes nearly identical to the ideal signal desired out of the receiver. Once this is achieved, the time delay coefficients vector for calibration, $\hat{\boldsymbol{T}}^{*}$, takes values of the approximated vector of time delays from the output of the algorithm, $\hat{\boldsymbol{T}}_k$, which is acquired from the final iteration when the convergence condition is met.

Based on the coefficients selection procedure described in the last subsection, the quasi-optimal coefficients for the algorithm were given in Table IV when the number of elements in the arrays was M = $4, 16, \cdots, 128$. The range of time delay distortions (bounded by a hypothetical maximum time delay distortion) was assumed between -1 ns and 1 ns. In general the values for a_k, b_k, and c_k are suggested to decrease as the iteration number, k, increases in order to reach the convergence asymptotically. We found that they can also be assigned with predetermined small constant values, such as when M = 128, a_k = 0.1 and c_k = 0.01, the convergence condition ($l \leq 0.001$) can also be reached.

The implementation of the algorithm with the loss function defined by combination of power and correlation coefficient shows a faster convergence speed. The comparison of convergence rate using two loss function definitions is shown in Fig. 2. In the simulation, M = 128 and the range of time delay distortion in the 128 element channels was between -1 ns and 1 ns. All the coefficients were kept the same apart from calculation of the loss functions.

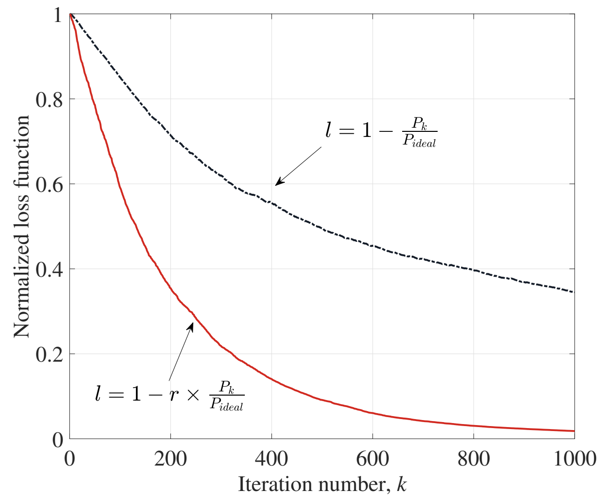

Fig. 2. Change of loss function as the iteration number, k, increases, when the number of elements in an array, $M = 128$. The range of time distortion in all element channels was assumed to be 2 ns. Comparison of changing trend of two loss functions, one is based on power measurement only, the other is based on combination of power and correlation coefficient calculation.

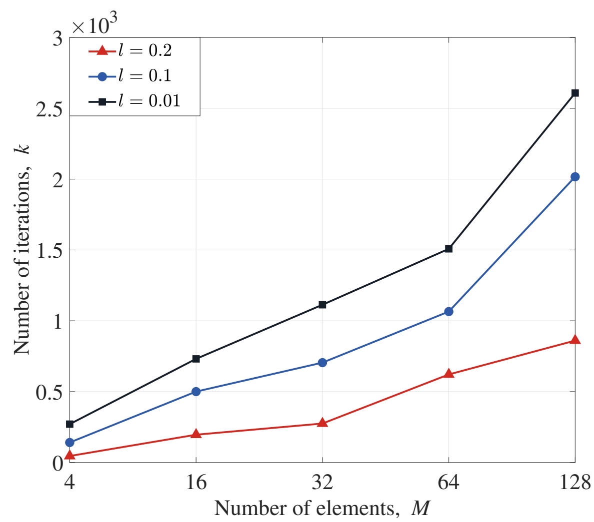

Fig. 3. The number of iterations required as a function of number of elements in the arrays, M. The loss function was based on combination of power measurement and correlation calculation, the range of time delay distortion in element channels is between -1 ns and 1 ns, the pulse signal used for calibration had w = 0.3, $\sigma_p^2 = 0.01$.

C. Analysis on number of iterations

The total number of iterations needed in the algorithm to reach the convergence depends on a number of factors: the assigned values for the initialization coefficients; the total number of array elements; level of accuracy the algorithm delivers. Number of iterations required to reach convergence as a function of number of elements in arrays for calibration

TABLE II
DATA SAMPLES FOR INITIALIZATION BEFORE ITERATIONS[1]

No. of $\boldsymbol{T}_0^*$	E1	E2	E3	E4	E5	E6	E7	E8	P_0	r_0	l_0	$\hat{g}_0$
1	0.2138	-0.9855	-0.4829	0.6891	-0.0196	-0.1323	0.7096	-0.6357	0.2156	0.0337	0.9927	0.3768
2	-0.1277	-0.9136	-0.3790	0.9645	0.3358	-0.1447	0.3567	0.2753	0.3692	-0.0923	1.0341	0.1763
3	0.1425	-0.5929	-0.2951	0.1826	0.0574	0.6398	0.1873	0.7278	0.4465	0.7579	0.6616	0.7781
4	0.3728	0.9498	-0.5444	0.7964	0.5095	0.9822	-0.1541	0.9457	0.4283	0.5206	0.7770	0.0984
5	0.3050	0.2493	-0.6987	-0.2373	0.1866	0.8946	-0.8270	0.1712	0.4253	0.3922	0.8332	0.3412
6	-0.5735	0.5929	-0.8724	0.8157	-0.3962	-0.4676	0.0639	-0.6066	0.3513	-0.6947	1.2440	0.0742
7	-0.6085	0.9997	0.5113	0.1124	-0.8132	-0.4586	-0.8509	-0.9373	0.1831	-0.5177	1.0948	0.1031
8	-0.4237	-0.4627	0.2106	0.8727	0.6507	-0.4322	-0.4856	-0.9527	0.2886	0.2558	0.9262	0.0892

[1]Random values for $\boldsymbol{T}_0^*$ were given 8 times, the magnitudes of power measurements, correlation coefficients, loss functions, and approximated gradients at early iterations were calculated, then were used to generate initialization coefficients for the SPSA algorithm, w = 0.3 and σ_p^2 = 0.01 for the Gaussian pulse.

TABLE III
DETERMINATION OF COEFFICIENTS FOR ITERATIONS[2]

Coefficient	α	γ	$\bar{\hat{g}}_0$	a_0	t_d	a	c	A
Value	0.602	0.101	0.2547	0.3926	0.1	1.4738	0.1865	8

[2]t_d is the desired change magnitude of time delays for compensation in early iterations, it was taken 5 percent of the range of time distortions (between -1 ns and 1 ns assumed in here), $t_d = a_0 \times \bar{\hat{g}}_0$, A is set to 8, a can then be derived based on (23) with $k = 0$, $a = a_0 \times (A+1)^\alpha$, c was taken as the standard deviation of l_0, i.e., $c = SD(l_0)$.

TABLE IV
QUASI-OPTIMAL COEFFICIENTS FOR THE ALGORITHM[3]

Scenario	$\bar{\hat{g}}_0$	a_0	t_d	a	c	A
$M = 4$	0.6937	0.1608	0.1	0.3798	0.2538	4
$M = 16$	0.4797	0.2370	0.1	1.3046	0.1625	16
$M = 32$	0.3571	0.3213	0.1	2.6367	0.1274	32
$M = 64$	0.2568	0.4649	0.1	5.7381	0.0882	64
$M = 128$	0.1533	0.7079	0.1	15.5301	0.0446	128

[3]The coefficients were calculated based on: the range of time delay distortions was assumed between -1 ns and 1 ns within each channel, the reference pulse signal used for calibration had $w = 0.3$, $\sigma_p^2 = 0.01$, and A is related to number of iterations, was given M.

under three convergence conditions ($l \leq 0.2$, $l \leq 0.1$ or $l \leq 0.01$) is given in Fig. 3. It indicated that number of iterations required increases significantly as the convergence condition becomes more stringent. The benefit of a smaller value as convergence condition was potentially compromised by number of iterations needed. Hence, a balance has to be sought. More novel gradient approximation approaches can be explored to accelerate the convergence, such as when the initial value of c and corresponding c_k are fixed, let b_k follow a polynomial delay, then a_k can be derived according to (25).

D. Analysis on accuracy of the algorithm

The accuracy of the algorithm is closely related to convergence condition. The ratio of discrepancy, between the intrinsic time delays (the hypothesized time delay distortions for real systems) $\boldsymbol{T}_{in}$ and the estimated time delays $\hat{\boldsymbol{T}}^*$, with the range of time distortions, is used as a measure for evaluating accuracy of the algorithm (mean$\{\|\hat{\boldsymbol{T}}^* - \boldsymbol{T}_{in}\|\}$/range$\{\boldsymbol{T}_{in}\}$). With the number of elements varying between 4 and 128, after the specified convergence was met ($l \leq 0.2$, $l \leq 0.1$ or $l \leq 0.01$), the corresponding estimation errors are shown in Fig. 4. It indicated that average estimation errors in arrays with different number of elements maintain a similar level as soon as the convergence condition is fixed. This can be better explained by observing the two particular cases (the insets) where the array had 4 and 128 elements respectively. When the convergence condition was met for each case (under $l \leq 0.01$), the estimation errors for all element channels distributed evenly of a similar magnitude (with 5% in error) despite the number of the elements in the arrays.

E. Receivers with true time delay

Wideband antenna arrays can be dealt with by adopting true time delay. Initially, switched delay lines were applied in the signal paths, and quantized delays were applied on the element or subarray levels. The recent developments of monolithic microwave integrated circuit (MMIC) chips introduce various amount of delays over a broad range of frequency. The

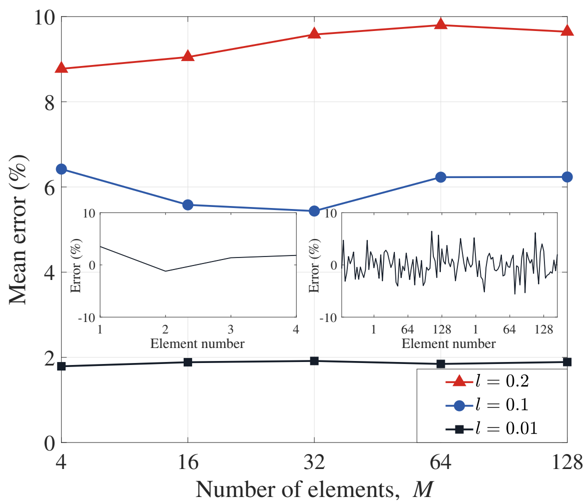

Fig. 4. The estimation error as the number of elements in arrays and convergence conditions vary. The estimation errors were averaged in all element channels and the ratio in percentage between the average time delay errors and the range of time distortions, 2 ns, were given. The inset on the left was for an array with 4 elements and the one on the right for an array with 128 elements. Both were converged when l was less than 0.01. The loss function was based on combination of power and correlation coefficient.

delay steps are controlled digitally with typical 8–12 bits. However, the range of time delays in a single chip is limited. Cascaded two-stage hybrid transmitter/receiver architecture is illustrated in Fig. 5. At present, the hybrid analog/digital configuration is preferred in practice to reduce the number of ADCs in wideband systems. Unlike the conventional quansi-monochromatic arrays where a digital beam can be steered by a simple assignment of phase and amplitude for each element at a single frequency, calibration must be carried out in the time domain for wideband arrays in order to balance the phase and amplitude over the entire bandwidth. Quantization on time delays may create errors as not the exact time delay offsets can be applied during iterations. The estimation was implemented with time delay steps controlled by an 8-bits circuit and the estimation error was compared with that using fully analog time delays in Fig. 6. The convergence ($l \leq 0.01$) was reached first with an analog time delay setting, then the same number of iteration was used in implementation with an 8-bits control circuit for time delay adjustment.

VI. Simulation Results

In order to validate the effectiveness of the proposed method, two scenarios have been considered to carry out calibration in the time domain on finite arrays. In the first scenario, it was assumed that the pulse transmitted for calibration was received without any changes in the element channels while in the second scenario, pulse distortion caused by transmitting and receiving was taken into consideration. Hence, the influence of pulse distortion on performance of the proposed calibration method was included in the study.

A. The unchanged pulses in the element channels

In order to illustrate how to carry out calibration in practice and verify its effectiveness in solving array calibration problems, the SPSA algorithm was adopted to carry out calibration on an aperture array with 16 elements in the time domain. The range of time delay distortion in each element channel is assumed between -1 ns and 1 ns. In the experiment, the loss function was defined by using the product of received power at the array output and the correlation coefficient between the received signal at the array output (with perturbated time delays in element channels) and the desired signal. The detailed flowchart of running the algorithm for the experiment is denoted in Fig. 7, where l was calculated based on (27) and evaluated against two convergence conditions (l reached 0.2 and 0.005 respectively) in each iteration.

The total number of elements in the array for calibration is set $M = 16$. A Gaussian pulse with the variance of $\sigma_p^2 = 0.01$ impinged onto the array from a far field, and the duration of time for the pulse is 1 ns. Initially, a time delay vector, $\boldsymbol{T}_{in}$ consisting of 16 elements was generated, of which each element was a random number distributed in the range between -1 and 1, representing time delays caused by element variation and imperfect channel condition. So the received signal from each element was defined as: $\boldsymbol{S}_1$=$\boldsymbol{s}(\boldsymbol{t}-\boldsymbol{T}_{in}(1))$, $\boldsymbol{S}_2$=$\boldsymbol{s}(\boldsymbol{t}-\boldsymbol{T}_{in}(2))$, $\cdots$, $\boldsymbol{S}_{16}$=$\boldsymbol{s}(\boldsymbol{t}-\boldsymbol{T}_{in}(16))$, the combined signal from the 16 channels prior to implementing the calibration procedure will be,

$$\boldsymbol{S}_{no\_cal} = \boldsymbol{S}_1 + \boldsymbol{S}_2 + \cdots + \boldsymbol{S}_{16}. \tag{28}$$

Approximated time delays were introduced in each channel for simultaneous perturbation, iterations were run through until the combined signal from the array output, with perturbation on time delay applied, was similar to the ideal signal (no time delays applied in element channels). When the convergence condition was met, the received signal from the array output was: $\boldsymbol{S}_{1\_c}$=$\boldsymbol{S}(\boldsymbol{t}-(\hat{\boldsymbol{T}}^*(1)-\boldsymbol{T}_{in}(1)))$, $\boldsymbol{S}_{2\_c}$=$\boldsymbol{S}(\boldsymbol{t}-(\hat{\boldsymbol{T}}^*(2)-\boldsymbol{T}_{in}(2)))$, $\cdots$, $\boldsymbol{S}_{16\_c}$=$\boldsymbol{S}(\boldsymbol{t}-(\hat{\boldsymbol{T}}^*(16)-\boldsymbol{T}_{in}(16)))$, and the combined signal can be expressed as,

$$\boldsymbol{S}_{calibrated} = \boldsymbol{S}_{1\_c} + \boldsymbol{S}_{2\_c} + \cdots + \boldsymbol{S}_{16\_c}. \tag{29}$$

During the intermediate steps of the optimization process, $\hat{\boldsymbol{T}}_k$ was renewed at each iteration by introducing time delay perturbation in each channel for the following step, the correlation coefficient between the received signal at the array output (with time delay perturbation in each element channel), $S_{calibrated}$, and the ideal signal at the array output (without time delays applied in each element channel) was used to establish the condition for convergence.

Initially, a time delay vector $\boldsymbol{T}_{in}$ with 16 elements was generated, a random value between -1 and 1 was assigned for each element to reflect the imperfect receiving condition of the array, and these are the time delays to be calibrated out of the system. The initial values of the $\boldsymbol{T}_{in}$, the time delay vector is given in Table V. As shown in Fig. 7, the SPSA algorithm itself has no prior information about these arbitrary values of time delays. It introduced time delays into channels

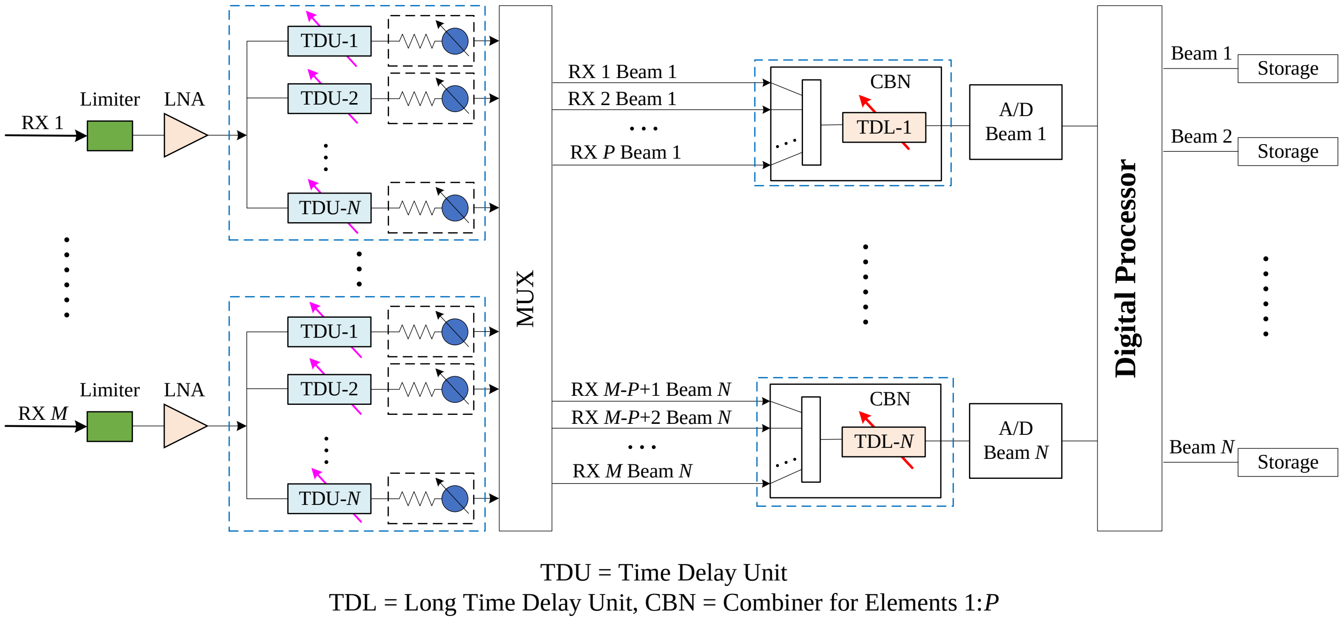

(a) Hybrid analog/digital receiver architecture

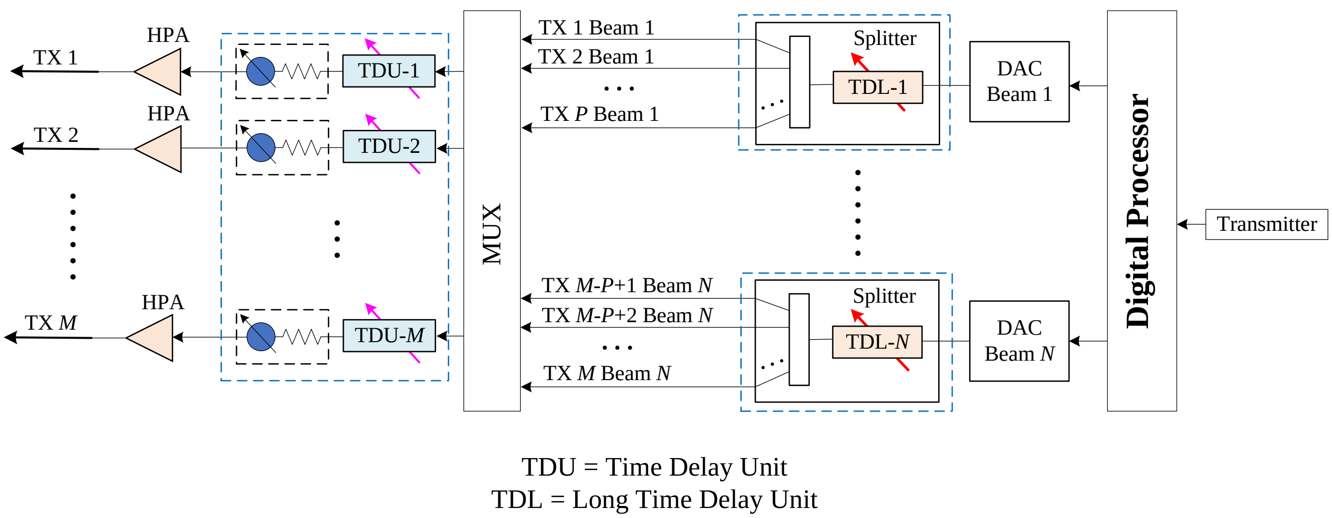

(b) Multibeam analog/digital transmitter architecture

Fig. 5. Hybrid multibeam analog/digital architecture with true time delay. (a) The multibeam configuration for receive with true time delay. (b) The transmit configuration with true time delay.

at each iteration and carry out measurement at the array output. Once the synthesized signal (based on the estimated delay corrections from the algorithm) has a close enough correlation with the combined signals (based on the random time delays at the beginning), i.e., the correlation coefficient between them is greater than a set value, the convergence criterion was met and the time delay vector, $\hat{\boldsymbol{T}}^{*}$, from the last iteration is the time delays to be used to make time delay adjustments. The synthesized signals based on $\boldsymbol{T}_{in}$ before and after calibration are compared in Fig. 8. The time delays for all receiving channels are to be compensated based on $\hat{\boldsymbol{T}}^{*}$, and they are used to cancel $\boldsymbol{T}_{in}$. The approximated values of $\hat{\boldsymbol{T}}^{*}$ from the algorithm were compared to the intrinsic time delays randomly generated in the array system at the beginning of calibration in Table V, the estimation error is much lower than 0.01 ns when the range of time deviation is between -1 ns and 1 ns, which verified the effectiveness of the proposed method.

B. The distorted pulses in the element channels

In practice, the pulses used for calibration will inevitably be distorted to some extent due to limitations in the antenna array and frequency-dependent fading during propagation. Hence, it is necessary to take the signal distortion effects into considerations during calibration. In order to verify the effectiveness of the proposed method under such circumstances, three examples have been demonstrated by implementing the proposed method: 1) A Gaussian pulse as defined in (10) was used as the reference signal ($w = 0.3$, $\sigma_p^2 = 0.01$)

TABLE V
EXPERIMENTAL RESULTS FOR THE ARRAY WITH 16 ELEMENTS

Array Element No. m	Intrinsic time delay $\boldsymbol{T}_{in}$ (ns)	SPSA, $l = 0.2$ Approx. delay $\hat{\boldsymbol{T}}^*$ (ns)	SPSA, $l = 0.2$ Approx. delay error (ns)	SPSA, $l = 0.005$ Approx. delay $\hat{\boldsymbol{T}}^*$ (ns)	SPSA, $l = 0.005$ Approx. delay error (ns)
1	-0.7222	-0.6780	-0.0442	-0.7188	-0.0034
2	-0.3305	-0.3288	-0.0017	-0.3309	0.0004
3	-0.9352	-0.9103	-0.0249	-0.9342	-0.0010
4	-0.3615	0.4067	-0.7682	-0.3613	-0.0002
5	0.3188	0.2876	-0.0312	0.3182	0.0006
6	0.2325	0.3209	-0.0884	0.2335	-0.0010
7	-0.4646	-0.4256	-0.0390	-0.4663	0.0017
8	-0.7118	-0.6931	-0.0187	-0.7118	0.0000
9	0.1604	0.1812	-0.0208	0.1613	-0.0009
10	0.6035	0.5742	0.0293	0.6041	-0.0006
11	-0.1765	-0.1834	0.0069	-0.1769	0.0004
12	0.4353	0.4159	0.0194	0.4348	0.0005
13	0.2565	0.1171	0.1394	0.2577	-0.0012
14	0.4433	0.3986	0.0447	0.4452	-0.0019
15	0.5461	0.4258	0.1203	0.5461	0.0000
16	0.2556	0.2574	-0.0018	0.2562	-0.0006

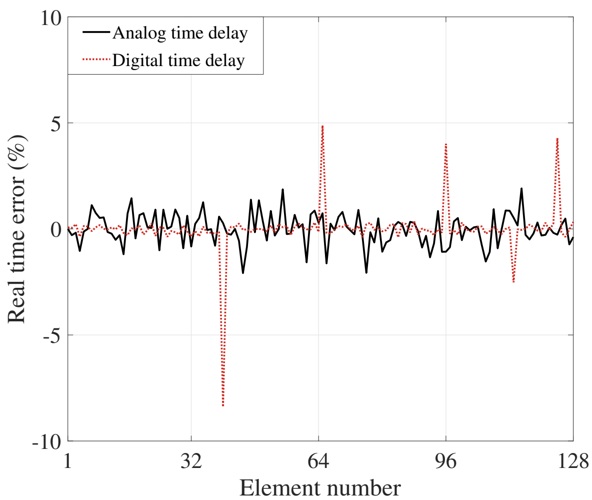

Fig. 6. Real time delay errors from estimation in each channel of the array with 128 elements, the algorithm was implemented with and without quantization on the time steps for adjustment. The y-axis value was calculated by $\{\hat{\boldsymbol{T}}^* - \boldsymbol{T}_{in}\}/\text{range}(\boldsymbol{T}_{in})$. The array had 128 elements with a range of 2 ns time distortions (between -1 ns and 1 ns) in each channel, the estimation was first run without quantization on time delays, after reaching convergence, the same number of iterations was used for estimation by a quantization scheme on the 2 ns range with 8 bits.

TABLE VI
COMPARISON OF CALIBRATION PERFORMANCE

Method	Distortion range	Domain	Accuracy (%)
Adapt [17], [37]	$(-5.625°, +5.625°)$	FD	89
Perturbation [19]	$(-32°, +32°)$	FD	95
REV [16]	$(-180°, +180°)$	FD	92
This work	$(-0.5$ ns, $+0.5$ ns$)$	TD	99.7

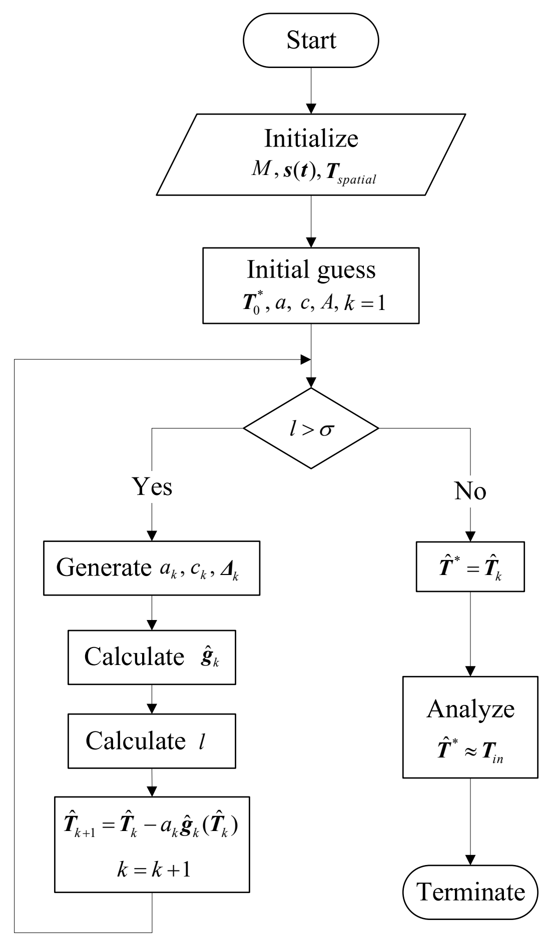

Fig. 7. The flowchart of the SPSA based methodology for aperture array calibration in the time domain.

and the received signals from the element channels had a similar form but with different variance values (σ_p^2 varying between 0.0217 and 0.0625) representing distortion effect in different element channels; 2) The Richard wavelet, the second derivative of the Gaussian pulse as in (10), $\boldsymbol{s}(\boldsymbol{t}) = 2A_m(2\alpha^2(\boldsymbol{t}-t_o)^2-\alpha)e^{(-\alpha(\boldsymbol{t}-t_o)^2)}$, was used as the reference signal (α=24) for calibration, whereas the pulses received from element channels used wavelets of different α values

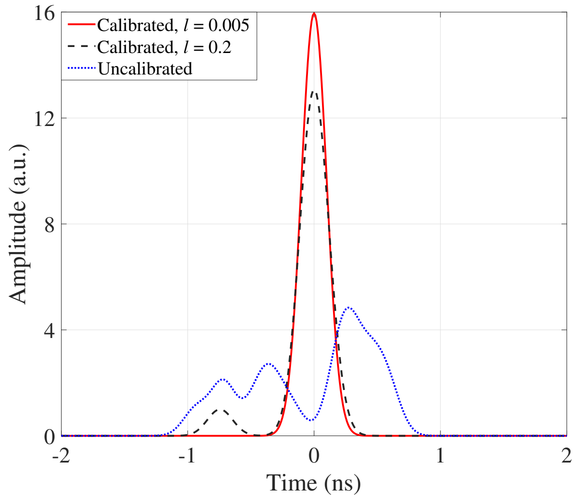

Fig. 8. The synthesized signal from the receiving channels for the 16 elements using a random time delay for each channel ($\boldsymbol{T}_{in}$) representing imperfect receiving condition and the time delay approximated for each channel from the algorithm ($\hat{\boldsymbol{T}}^{*}$) for calibration.

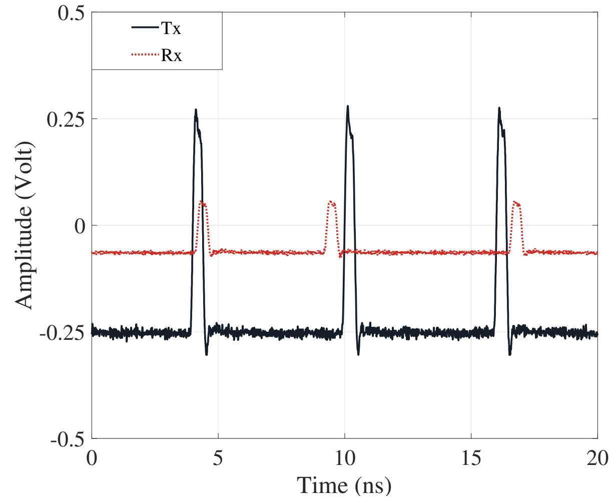

(a) The transmitted and received pulses in the time domain

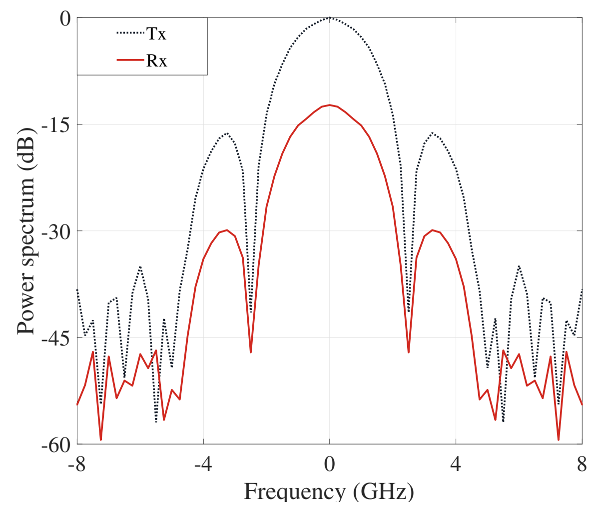

(b) The power spectrum of the real pulse

Fig. 9. The illustration of pulses transmitted, the reference pulse waveform for calibration, and the received pulses from a power splitter emulating the pulses received from the element channels, and the source pulse from AWG5204 has a width of 400 ps. (a) The transmitted and received pulses in the time domain, the repetitive pulses at the transmit side was shown giving an indication of a regular interval where the received pulses were deviated from the regular intervals, the time deviations are to be calibrated; (b) The power spectrum of the transmitted and received pulses.

(α varying between 8 and 23 for the 16 elements); 3) Finally, the short pulse signal was generated from the signal generator AWG5204 (from Tektronix) with the pulse width of 400 ps in the setting, the received pulses were taken from the output ports of the power splitter where the random propagation delay in each channel was introduced later on after the respective pulse waveforms were collected. The transmitted pulse and the received pulses in the time domain and frequency domain are shown in Fig. 9. It can be seen that the pulse waveform was modified during propagation and this was more clearly observed in the frequency domain. The imperfect array antenna condition was further illustrated by the phenomenon that the received pulses were not showing up in an regular interval. The source pulse was used as a reference signal to launch the algorithm with the above-mentioned received pulse distributing among the element channels with random time delays. The calibration results for the three examples mentioned above are given in Fig. 10. It indicated that the accuracy of the time delays estimated is better than 99% even though the pulses received from the element channels were different with the reference pulse waveform for calibration. The calibration performance was compared with other typical calibration methods performed in the frequency domain, and the main parameters are summarized in Table VI.

VII. Discussions

An idealized solution to the general problem of calibration is to determine a number of unknowns (presumably constant over a period of time at least) from a minimum number of measured quantities (independent to each other.) In an broadband aperture array with a large number of elements, number of measurements required to resolve calibration coefficients is significant and difficult to implement practically, in particular expensive near field facility testing is infeasible for arrays with large dimensions. The method based on time domain operations presented in this paper is an attempt to cope with these challenges. The accurate calibration of aperture array antennas does not require the full capability of an near-field range (NFR) facility to physically sample the RF field in front of the array in half wavelength increments, or the response of each radiating element as is required in most existing calibration methods.

The characteristic of the short pulse employed for calibration has a connection with the operational frequency band of aperture arrays. It should be decided following the principle that a minimum distortion is caused to the pulse while receiving from the array elements. However, filtering effect of array antennas on the signal for calibration can be mitigated by using the pulse signal received from an array element as the

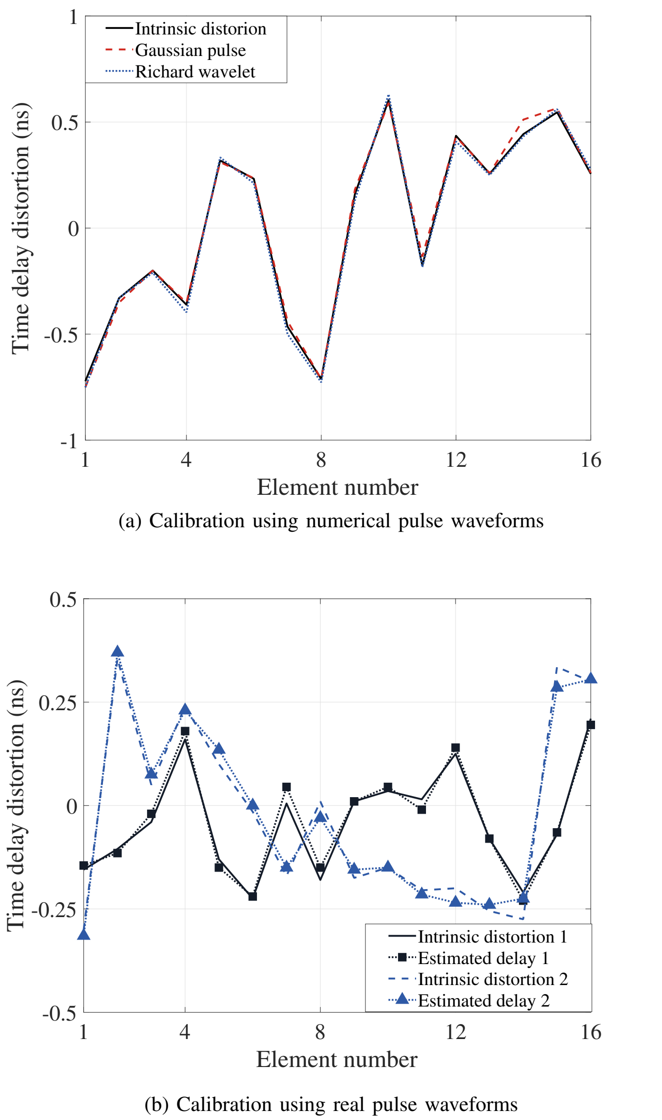

Fig. 10. The calibration performance when the received pulses in the element channels were different to the reference pulse. Two sets of random delays for 16 element channels were used for verification, they were defined as case 1 and case 2 respectively. (a) The reference pulse for calibration is a Gaussian pulse or a Richard wavelet, and the received pulses in the element channels were different to the reference pulses; (b) The reference pulse is the pulse generated from the signal generator with the pulse width of 400 ps, the received pulses in the element channels were distorted and therefore different with the reference pulse.

reference signal. The algorithm can cope with pulse distortions without a significant compromise on estimation performance as shown in Fig. 10 where distorted pulses from array elements were considered during calibration.

The same method can be applied in the frequency domain by changing the signal for calibration from a short pulse to a narrow-band signal in order to determine optimal phase offset coefficients in element channels. The loss function defined in (19) can be adopted. As this is not the focus of this paper, we do not elaborate further on this. But we note a very high level of accuracy can be achieved if the method is implemented in the frequency domain using such method.

Aperture array technology is evolving with advances in solid-state microwave integrated circuits. Element-level digital beamforming (DBF) becomes increasingly realistic. However, digital subarray architecture represents a feasible compromise between the number of beams and the number of digital channels. For such arrays as illustrated in Fig. 5, the algorithm can be launched in each subarray, it can also be applied to make time delay compensations between the subarrays before beams from subarrays being digitized.

For most time delay RFICs, adjustable delay range is between 0 ps and 200 ps. The state-of-the-art MMICs has a maximum time delay in the order of 1000 ps covering various frequency bands. The maximum time distortion in element channels the algorithm dealt with was 2000 ps (between -1 ns and 1ns) in the analysis. However, the time delay range can be adjusted based on practical needs. The number of iterations will reduce when the range of time delay distortions occurring in array element channels is smaller as it is easier to converge.

It is worth mentioning that the method proposed in this work is applicable for calibration of broadband antenna arrays employing time delay units at the element or subarray level. Before the utilization of fully digitized antenna arrays becomes more accessible, broadband array systems with true time delays (TTDs) are being developed to mitigate or eliminate "squint" phenomenon by adopting phased-steered approaches for scanning, which works well for a system with a narrow radio-frequency bandwidth. However, for applications where high resolution is desired such as imaging and tracking, more radical changes in technology including integrated circuits of TTD with a higher time delay resolution, such as 8–12-bits time delay shifters, are expected. These higher cost systems are needed to provide the performance requirements for high resolution applications and the calibration method proposed in this work can greatly reduce the complexity of calibrating such systems. Various antenna array architecture solutions with integrated TTD units are presented in [45].

In practice, quantization step size of TTDs plays an important role on the accuracy of the proposed method. When the number of control bits for the time delay shifter reduces, the calibration error will rise as the accurate time delay coefficients in element channels are more difficult to acquire and this leads to ambiguity. One reference case has been examined in the previous discussion where the errors of time delay coefficients for calibration at several element channels (in an array with 128 elements) are approximately 10% with 8-bits resolution TTD units.

Antenna arrays can have complex and extended time domain responses—impulse responses, that have the potential to significantly alter the transmitted or received waveforms, either because of the environment or the array itself. On the other hand, by using phase shifters, a significant squint-induced broadening on the main beam will occur when the array has a wide bandwidth, hence TTDs have to be adopted to restore beamwidth performance. The required TTD, $\varDelta T$, and phase shift, $\varDelta\varphi$, have the following relation,

$$\varDelta T = \frac{\varDelta\varphi}{2\pi f} = \frac{d sin(\theta)}{c}. \quad (30)$$

For a broadband waveform with a pulse width in time $\tau_p \ll$

$Mdsin(\theta)/c$, even if dispersion exists in the Tx/Rx paths, which occurs because of the reflections or other effects, as the time resolution is high, the responses irrelevant to calibration can be filtered out in the time domain. In addition, the settings used for calibration are mainly considered to be under line of sight (LOS) propagation.

As mentioned in Section VI-B, the pulse shapes with distortion due to transmitting, propagation and receiving have a minor effect on calibration performance as soon as the reference pulse signal for calibration is narrow enough compared to the maximum time delay distortion occurring in the element channels. This suggests that the suitable pulse waveform can be chosen based on the following principles: 1) the time domain waveform covers the 3 dB bandwidth of the operational frequency of the array; 2) the duration of the pulse is significantly less than the maximum time delay distortion in the element channels. One approach can be achieved by measuring the impulse response of one element in the array, then using this impulse response as the reference pulse for calibration, where a vector network analyzer with time-domain transforming capability can be used.

VIII. Conclusion

A new calibration method for aperture arrays in the time domain has been proposed. It exploits the stochastic approximation algorithm with simultaneous perturbation. The proposed method can be successfully applied for calibrating antenna arrays of ultrawide bandwidth in the time domain. The main contributions of the paper can be summarized as follows: 1) It gives the technical details of recurrence relation needed to implement the algorithm for the purpose of array calibration in the time domain and the strategy on selecting the initial values of the coefficients to start the algorithm; 2) It demonstrates that two types of loss functions can be employed to establish the convergence criterion based on the availability in practice; 3) It provides guidance for the optimal values of the coefficients, and their relationship with the problem; 4) Small arrays or large arrays can be treated in different tiers by assigning different values for coefficients; 5) It shows that the convergence can be reached at ease to ensure an estimation error within $\pm 1\%$ of the total time duration of the short pulse that was employed for calibration. This validated the efficacy of the method for calibrating aperture arrays and opens new options for online calibration of ultra-wideband arrays without the need for resorting to expensive and time-consuming near field facility testing. It holds great potential for millimeter or THz applications where increased frequency bandwidth and real-time processing is in need.

The scope of the method is for array systems with TTD units at the element or subarray level, where the time resolution is high and it should be significantly smaller than the maximum time distortion occurring in the element channels. The future work includes waveform design for optimal calibration performance, and apply the proposed method for wideband beamforming under more complex situations.

References

[1] H. Bui-Van, J. Abraham, M. Arts, Q. Gueuning, C. Raucy, D. González-Ovejero, E. de Lera Acedo, and C. Craeye, "Fast and accurate simulation technique for large irregular arrays," *IEEE Trans. Antennas Propag.*, vol. 66, no. 4, pp. 1805–1817, Feb. 2018.

[2] T. Moon, J. Gaun, and H. Hassanieh, "Know your channel first, then calibrate your mmwave phased array," *IEEE Des. Test*, vol. 37, no. 4, pp. 42–51, Jul. 2020.

[3] N. Tyler, B. Allen, and H. Aghvami, "Adaptive antennas: the calibration problem," *IEEE Commun. Mag.*, vol. 42, no. 12, pp. 114–122, Dec. 2004.

[4] B. Friedland, "On the calibration problem," *IEEE Trans. Autom. Control*, vol. 22, no. 6, pp. 899–905, Dec. 1977.

[5] J. J. Schuss, T. V. Sikina, J. E. Hilliard, P. J. Makridakis, J. Upton, J. C. Yeh, and S. M. Sparagna, "Large-scale phased array calibration," *IEEE Trans. Antennas Propag.*, vol. 67, no. 9, pp. 5919–5933, Sep. 2019.

[6] K. F. Warnick, R. Maaskant, M. V. Ivashina, D. B. Davidson, and B. D. Jeffs, "High-sensitivity phased array receivers for radio astronomy," *Proc. IEEE*, vol. 104, no. 3, pp. 607–622, Feb. 2016.

[7] M. A. Salas-Natera, R. M. Rodriguez-Osorio, and L. de Haro, "Procedure for measurement, characterization, and calibration of active antenna arrays," *IEEE Trans. Instrum. Meas.*, vol. 62, no. 2, pp. 377–391, Feb. 2013.

[8] R. Maaskant, M. V. Ivashina, S. J. Wijnholds, and K. F. Warnick, "Efficient prediction of array element patterns using physics-based expansions and a single far-field measurement," *IEEE Trans. Antennas Propag.*, vol. 60, no. 8, pp. 3614–3621, May 2012.

[9] M. Leavitt, "A phase adaptation algorithm," *IEEE Trans. Antennas Propag.*, vol. 24, no. 5, pp. 754–756, Sep. 1976.

[10] J. C. Spall, "Multivariate stochastic approximation using a simultaneous perturbation gradient approximation," *IEEE Trans. Autom. Control*, vol. 37, no. 3, pp. 332–341, Mar. 1992.

[11] ——, "Implementation of the simultaneous perturbation algorithm for stochastic optimization," *IEEE Trans. Aerosp. Electron. Syst.*, vol. 34, no. 3, pp. 817–823, Jul. 1998.

[12] ——, "Adaptive stochastic approximation by the simultaneous perturbation method," *IEEE Trans. Autom. Control*, vol. 45, no. 10, pp. 1839–1853, Oct. 2000.

[13] O. Granichin and N. Amelina, "Simultaneous perturbation stochastic approximation for tracking under unknown but bounded disturbances," *IEEE Trans. Autom. Control*, vol. 60, no. 6, pp. 1653–1658, Sep. 2015.

[14] O. Granichin, V. Erofeeva, Y. Ivanskiy, and Y. Jiang, "Simultaneous perturbation stochastic approximation-based consensus for tracking under unknown-but-bounded disturbances," *IEEE Trans. Autom. Control*, vol. 66, no. 8, pp. 3710–3717, Sep. 2021.

[15] T. Takahashi, Y. Konishi, S. Makino, H. Ohmine, and H. Nakaguro, "Fast measurement technique for phased array calibration," *IEEE Trans. Antennas Propag.*, vol. 56, no. 7, pp. 1888–1899, Jul. 2008.

[16] T. Takahashi, Y. Konishi, and I. Chiba, "A novel amplitude-only measurement method to determine element fields in phased arrays," *IEEE Trans. Antennas Propag.*, vol. 60, no. 7, pp. 3222–3230, Jul. 2012.

[17] R. Sorace, "Phased array calibration," *IEEE Trans. Antennas Propag.*, vol. 49, no. 4, pp. 517–525, Apr. 2001.

[18] V. I. Djigan and V. V. Kurganov, "Antenna array calibration algorithm based on phase perturbation," *2019 IEEE East-West Design Test Symposium (EWDTS)*, pp. 1–5, Nov. 2019.

[19] ——, "Antenna array calibration algorithm without access to channel signals," *Radioelectron. Commun. Syst.*, vol. 63, no. 1, pp. 3–20, Mar. 2020.

[20] S. Mano and T. Katagi, "A method for measuring amplitude and phase of each radiating element of a phased array antenna," *Electron. Commun. Jpn.*, vol. 65-B, no. 5, pp. 58–64, Mar. 1982.

[21] L. Prashanth, S. Bhatnagar, N. Bhavsar, M. Fu, and S. I. Marcus, "Random directions stochastic approximation with deterministic perturbations," *IEEE Trans. Autom. Control*, vol. 65, no. 6, pp. 2450–2465, Jul. 2020.

[22] A. Agrawal and A. Jablon, "A calibration technique for active phased array antennas," *IEEE Int Symp Phased Array Syst Technol.*, pp. 223–228, Jan. 2003.

[23] Y. V. Korotetskiy, A. M. Shitikov, and V. V. Denisenko, "Phased array antenna calibration problems, including in-service and multi-element paa calibration," *Int. Conf. Antenna Theory Tech (ICATT)*, pp. 405–407, Sep. 2013.

[24] S. V. Elizarov, D. S. Smirnov, Y. A. Suserov, E. V. Korotetskiy, and A. M. Shitikov, "Calibration and measurements of large multi-element array

antennas," *Conf. Proc. - Radiat. Scatt. Electromagn. Waves (RSEMW)*, pp. 395–396, Nov. 2017.

[25] M. D. Migliore, "A compressed sensing approach for array diagnosis from a small set of near-field measurements," *IEEE Trans. Antennas Propag.*, vol. 59, no. 6, pp. 2127–2133, Apr. 2011.

[26] H.-T. Chou, J. W. Liu, and W.-J. Liao, "Eur. conf. antennas propag (eucap)," *2019 13th European Conference on Antennas and Propagation (EuCAP)*, pp. 1–4, Mar. 2019.

[27] R. Mailloux, *Phased Array Antenna Handbook*, 3rd ed. Boston and London: Artech House, Inc, 2018, ch. 7.

[28] H. M. Aumann, A. J. Fenn, and F. G. Willwerth, "Phased array antenna calibration and pattern prediction using mutual coupling measurements," *IEEE Trans. on Antennas Propag.*, vol. 37, no. 7, pp. 844–850, Jul. 1989.

[29] C. Shipley and D. Woods, "Mutual coupling-based calibration of phased array antennas," *IEEE Int. Symp. Phased Array Syst. Technol.*, pp. 529–532, May 2000.

[30] K.-M. Lee, R.-S. Chu, and S.-C. Liu, "A built-in performance-monitoring/fault isolation and correction (pm/fic) system for active phased-array antennas," *IEEE Trans. Antennas Propag.*, vol. 41, no. 11, pp. 1530–1540, Nov. 1993.

[31] G. Hampson and A. Smolders, "Ieee antennas propag. soc. int. symp.: Wirel. technol. inf. netw., aps - held conjunction usnc/ursi national radio sci. meet." *IEEE Antennas and Propagation Society International Symposium. 1999 Digest. Held in conjunction with: USNC/URSI National Radio Science Meeting (Cat. No.99CH37010)*, vol. 2, pp. 1040–1043, Jul. 1999.

[32] R. Yonezawa, Y. Konishi, I. Chiba, and T. Katagi, "Beam-shape correction in deployable phased arrays," *IEEE Trans. Antennas Propag.*, vol. 47, no. 3, pp. 482–486, Mar. 1999.

[33] T. Takahashi, H. Miyashita, Y. Konishi, and S. Makino, "Theoretical study on measurement accuracy of rotating element electric field vector (rev) method," *Electron. Commun. Jpn. (Part I: Communications)*, vol. 89, no. 1, pp. 22–33, Sep. 2006.

[34] M. Liu and Z. Feng, "Calibration of large scale phased array antennas by packet rotation vector method," *J. Radio Sci.*, vol. 22, no. 03, pp. 380–384, Mar. 2007.

[35] H.-J. Yoon and B.-W. Min, "Improved rotating-element electric-field vector method for fast far-field phased array calibration," *IEEE Trans. Antennas Propag.*, vol. 69, no. 11, pp. 8021–8026, Jun. 2021.

[36] H. Steyskal, R. Shore, and R. Haupt, "Methods for null control and their effects on the radiation pattern," *IEEE Trans. Antennas Propag.*, vol. 34, no. 3, pp. 404–409, Mar. 1986.

[37] H. Wang and H. Sun, "Fast calibration method for phased array antenna," *Journal of Beijing University of Aeronautics and Astronautics*, vol. 42, no. 12, pp. 2709–2714, Dec. 2016.

[38] R. Long, J. Ouyang, F. Yang, W. Han, and L. Zhou, "Fast amplitude-only measurement method for phased array calibration," *IEEE Trans. Antennas Propag.*, vol. 65, no. 4, pp. 1815–1822, Nov. 2017.

[39] Q. Gueuning, A. K. Brown, C. Craey, and E. d. L. Acedo, "A beam-forming approach to the self-calibration of phased arrays," *Eur. Conf. Antennas Propag (EuCAP)*, pp. 1–4, Mar. 2020.

[40] A. Nafe, K. Kibaroglu, M. Sayginer, and G. M. Rebeiz, "An in-situ self-test and self-calibration technique utilizing antenna mutual coupling for 5g multi-beam trx phased arrays," *IEEE MTT-S Int. Microwave Symp. Dig. (IMS)*, pp. 1229–1232, Jun. 2019.

[41] G. Babur, D. Caratelli, and A. Mirmanov, "Phased antenna array calibration based on compressed sensing theory," *IEEE Antennas Propag. Soc. Int. Symp. USNC/URSI Natl. Radio Sci. Meet. (APSURSI - Proc.)*, pp. 2213–2214, Jul. 2018.

[42] T. Tan, D. Chen, Y. Xue, and J. Zhuang, "Compressive-sensing-based antenna array calibration with manifold separation technique," *IEEE Int. Conf. Comput. Commun. (ICCC)*, pp. 453–457, Dec. 2020.

[43] H. J. Kushner and G. G. Yin, *Stochastic Approximation and Recursive Algorithms and Applications*, 2nd ed. New York: Springer New York, NY, 2003, ch. 1.

[44] J. C. Spall, *Introduction to Stochastic Search and Optimization. Estimation, Simulation, and Control*. New York: John Wiley & Sons, Ltd, 2003, ch. 7.

[45] R. Rotman, M. Tur, and L. Yaron, "True time delay in phased arrays," *Proc. IEEE*, vol. 104, no. 3, pp. 504–518, 2016.